International Journal of Solids and Structures 48 (2011) 3011–3019

Contents lists available at ScienceDirect

International Journal of Solids and Structures

journal homepage: www.elsevier.com/locate/ijsolstr

Optimal design of trusses with geometric imperfections: Accounting for global instability

Mehdi Jalalpour, Takeru Igusa, James K. Guest *

Department of Civil Engineering, Johns Hopkins University, Baltimore, MD 21218, United States

ARTICLE INFO

Article history:
Received 11 April 2011
Received in revised form 20 June 2011
Available online 1 July 2011

Keywords:
Topology optimization
Robust design
Global stability
Geometric imperfections
Buckling
Geometric uncertainties
Perturbation

ABSTRACT

A topology optimization method is proposed for the design of trusses with random geometric imperfections due to fabrication errors. This method is a generalization of a previously developed perturbation approach to topology optimization under geometric uncertainties. The main novelty in the present paper is that the objective function includes the nonlinear effects of potential buckling due to misaligned structural members. Solutions are therefore dependent on the magnitude of applied loads and the direction of resulting internal member forces (whether they are compression or tension). Direct differentiation is used in the sensitivity analysis, and analytical expressions for the associated derivatives are derived in a form that is computationally efficient. A series of examples illustrate how the effects of geometric imperfections and buckling may have substantial influence on truss design. Monte Carlo simulation together with second-order elastic analysis is used to verify that solutions offer improved performance in the presence of geometric uncertainties.

1. Introduction

Structural optimization offers a systematic approach to material layout in engineering design. Its most general branch is topology optimization where both structural component sizes and system connectivity are simultaneously optimized (Bendsøe and Sigmund, 2003). Structural optimization naturally drives design towards sparse and slender structures. Such structures are typically more susceptible to the deleterious effects of fabrication errors, including decreased resistance to buckling in the presence of geometric imperfections. This work presents a topology optimization algorithm that includes the effects of geometric variability in the manufacturing process, with the goal of improving design robustness. We focus on truss structures, and extend a recently developed perturbation-based approach (Guest and Igusa, 2008; Asadpoure et al., 2011) by accounting for nonlinear structural behavior.

Truss topology optimization typically follows a ground structure approach. The design domain is discretized with a nodal mesh that is connected by a dense set of potential structural members. Boundary conditions and applied loads are assumed known, and optimization is used to determine the distribution of cross-sectional areas (Kirsch, 1989; Bendsøe et al., 1994; Achtziger et al., 1992; Bendsøe and Sigmund, 2003). Members with areas below a certain threshold are deemed inefficient and are removed from the ground structure, thereby changing connectivity of the system.

There exists a rich literature on the design of trusses using optimization. We are concerned here with those works that are related to buckling. This area has recently generated significant interest among researchers due to technological advancements, including improved material strengths and manufacturing capabilities, that allow for design of more slender structural components. Buckling can be viewed as a combination of local (Euler) and global (system) buckling. One natural approach for developing designs that resist local buckling is to include the Euler buckling criterion in the constraints (Neves et al., 1995; Stolpe, 2004). However this formulation poses several fundamental and numerical challenges (Duysinx and Bendsøe, 1998; Kirsch, 1996; Zhou, 1996). Guo et al. (2001), for example, describe how this formulation may lead to a division of the feasible domain into disjoint subdomains, with the optimal solutions at the boundaries making them difficult locate with conventional optimizers. Cheng and Guo (1997) proposed the method of epsilon relaxation to overcome a similar difficulty.

While these methods account for the effects of local buckling, solutions can still be globally unstable, as in the common case of a chain of collinearly connected elements. While these collinear elements can be merged into one longer element through a method known as node cancelation, Zhou (1996) demonstrated that this increases the potential for Euler buckling, leading to suboptimal solutions. Achtziger (1999) circumvented this using local buckling constraints that account for the node cancelation effect via an exact

* Corresponding author.
E-mail address: jkguest@jhu.edu (J.K. Guest).

0020-7683/$ - see front matter © 2011 Elsevier Ltd. All rights reserved.
doi:10.1016/j.ijsolstr.2011.06.020

modeling method to consider the full length of isolated collinear chains. In terms of global buckling, Guo et al. (2005) attempt to circumvent collinear chains by using overlapping members in the ground structure while Rozvany (1996) explored the use of system stability constraints and geometric imperfections to facilitate creation of the kind of bracing needed to prevent global buckling behavior. Ben-Tal and Nemirovski (1997) proposed using artificial nodal loads to stabilize the system, which Tyas et al. (2006) updated with a scaling based on the internal force magnitudes of the members connected to the node. Ben-Tal et al. (2000) and Kočvara (2002) formulated an approach for deterministic truss design that included linearized global buckling in the compliance formulation.

As suggested by the works in the preceding paragraphs, topology optimization often exhibits numerical challenges associated with the underlying governing mechanics, such as local and global instability. Hence, topology optimization research has focused primarily on deterministic design problems, with the inclusion of uncertainty typically limited to the loading, treated probabilistically or through multiple load cases (Bendsøe et al., 1994; Diaz and Bendsøe, 1992; Lógó, 2007; Lógó et al., 2009; Yonekura and Kanno, 2010). Uncertainties associated with structural stiffness, however, can be important in design. This is particularly true in optimized structures that tend to be light, slender and sensitive to uncertainties in geometric and material properties. In the presence of such uncertainties, the global stiffness matrix becomes a random matrix, complicating the sensitivity analysis. Sandgren and Cameron (2002) circumvented this by taking a simulation-based approach, using a genetic algorithm as the optimizer and Monte Carlo simulation to represent uncertainties in geometry and material properties. Calafiore and Dabbene (2008) proposed relaxed approximations to the formulation to optimize under the condition of material property randomness.

The work herein follows a recently proposed method for structural optimization considering small uncertainty in nodal locations (Guest and Igusa, 2008) and/or material properties (Asadpoure et al., 2011). This method used second-order perturbations of the stiffness matrix to transform the uncertainties in nodal locations to a set of mathematically equivalent random forces. Although similar in concept to the aforementioned work of Ben-Tal and Nemirovski (1997) and Tyas et al. (2006), the method is unique in that the loads were a pure mathematical transformation of the uncertainty and that the design sensitivity analysis accounted for this transformation, allowing joints with uncertain location to being removed or braced in final designs. The perturbations, however, were based on linear elastic structural behavior; thus, the optimized designs were invariant to the magnitude and direction of the load. The current work extends this method by introducing first-order nonlinear effects associated with buckling so that the final resulting material distributions will be different under compressive and tensile forces. In this manner, the newly proposed method is capable of handling both nodal location uncertainty and, to first order, global buckling effects. To the best of the authors' knowledge, such a method does not exist in the literature.

This paper is structured as follows. The expected (mean) compliance is derived for a truss structure with imperfections in nodal locations and with potential global buckling. It is then shown how this compliance expression can be used in topology optimization. Finally, several design examples are presented, illustrating how the effects of geometric imperfections and global instability can result in substantial changes in the design.

2. Geometric imperfections

In this section we derive the formulations for converting the problem of trusses with geometric imperfections to an equivalent random forces problem. These are then extended to consider a first-order approximation to geometric nonlinearity. Applied loads are assumed deterministic. The detailed derivation that follows is general and applies to structures defined in any number of spatial dimensions having any number of nodal location uncertainties.

2.1. Expected value of the compliance

Structure geometry is defined by the node locations of the finite element discretization. Geometric uncertainties may then be represented by adding randomness to the spatial coordinates of the nodes. Mathematically, this is expressed as

$$X_i = X_{io} + \Delta X_i \tag{1}$$

where X_{i0} is the value of nodal coordinate i for the case where there is no geometric uncertainty and ΔX_i is the random variable that quantifies the uncertainty in this coordinate. The uncertainties ΔX_i are modeled as zero mean, uncorrelated random variables with variance $E\left[\Delta X_i^2\right] = \sigma_i^2$. Guest and Igusa (2008) showed that perturbation can be used to decompose the nodal uncertainties into a mathematically equivalent system of random loads. These equivalent random loads are associated with the first-order terms of the perturbation of stiffness matrix and are expressed as

$$\Delta\mathbf{f}^{(1)} = -\mathbf{K}_{0,i}\mathbf{d}\Delta X_i \tag{2}$$

Here, the bold lower- and upper-case letters represents vectors and matrices, respectively, and standard indicial notation is used, where repeated indices implies a summation. Also, $\mathbf{K}_0$ is the deterministic global stiffness matrix, the subscript $0,i$ indicates the derivative with respect to coordinate i, and $\mathbf{d}$ is the vector of displacements due to the applied loads $\mathbf{f}$. The superscript (1) used for the equivalent random load vector $\Delta\mathbf{f}^{(1)}$ is needed in the following discussion.

Herein, we extend the above, previously developed perturbation result by partially including the nonlinear effect of geometric imperfections. This is done by iteration. To initialize the iteration process, we use the magnitude of the nodal coordinate random variables as the original random displacements, given in vector form as

$$\Delta\mathbf{d}^{(0)} = \mathbf{e}_i\Delta X_i \tag{3}$$

where $\mathbf{e}_i$ is the unit vector associated with coordinate i. The first iteration for the random displacements would be the sum of this initial displacement field and the additional displacements due to the random forces $\Delta\mathbf{f}^{(1)}$:

$$\Delta\mathbf{d}^{(1)} = \Delta\mathbf{d}^{(0)} + \mathbf{K}_0^{-1}\Delta\mathbf{f}^{(1)} = \Delta\mathbf{d}^{(0)} - \mathbf{K}_0^{-1}\mathbf{K}_{0,i}\mathbf{d}\Delta X_i \tag{4}$$

in which we have used the expression for $\Delta\mathbf{f}^{(1)}$ from Eq. (2). This can be expressed in terms of the initial random displacement $\Delta\mathbf{d}^{(0)}$ by using the Kroneker delta, $\delta_{ij} = \mathbf{e}_i^{\mathrm{T}}\mathbf{e}_j$:

$$\Delta\mathbf{d}^{(1)} = \Delta\mathbf{d}^{(0)} - \mathbf{K}_0^{-1}\mathbf{K}_{0,i}\mathbf{d}\mathbf{e}_i^{\mathrm{T}}\mathbf{e}_j\Delta X_j = (\mathbf{I}+\mathbf{U})\Delta\mathbf{d}^{(0)} \tag{5}$$

where $\mathbf{I}$ is the identity matrix and

$$\mathbf{U} = -\mathbf{K}_0^{-1}\mathbf{K}_{0,i}\mathbf{d}\mathbf{e}_i^{\mathrm{T}} \tag{6}$$

is a dimensionless matrix. If this iteration process is continued, then we obtain, for iteration k

$$\Delta\mathbf{d}^{(k)} = (\mathbf{I}+\mathbf{U}+\cdots+\mathbf{U}^{\mathrm{k}})\Delta\mathbf{d}^{(0)} \tag{7}$$

with the limit for an infinite number of iterations given by:

$$\Delta\mathbf{d} = (\mathbf{I}-\mathbf{U})^{(-1)}\Delta\mathbf{d}^{(0)} = \mathbf{A}\Delta\mathbf{d}^{(0)} \tag{8}$$

where

$$\mathbf{A} = (\mathbf{I}-\mathbf{U})^{-1} \tag{9}$$

provided the inverse exists. The matrix $\mathbf{A}$ can be thought of as an amplification matrix as it essentially propagates the effect of a random variable through the structure. The equivalent force associated with this random displacement is simply an extension of Eq. (2):

$$\Delta\mathbf{f} = -\mathbf{K}_{0,i}\mathbf{d}\mathbf{e}_i^{\mathrm{T}}\Delta\mathbf{d} = \mathbf{K}_0\mathbf{U}\Delta\mathbf{d} \tag{10}$$

A standard approach in topology optimization is to maximize structural stiffness by minimizing external work done by the applied loads. This is commonly referred to as the minimum compliance design. Guest and Igusa (2008) showed that the expression for the compliance that includes the effects of geometric uncertainties up to second order is

$$c = \mathbf{f}^{\mathrm{T}}\mathbf{d} + \Delta\mathbf{f}^{\mathrm{T}}\mathbf{K}_0^{-1}\Delta\mathbf{f} - \frac{1}{2}\Delta d_i^{\mathrm{T}}\mathbf{d}^{\mathrm{T}}\mathbf{K}_{0,ij}\mathbf{d}\Delta d_j \tag{11}$$

where Δd_j is the jth component of the vector $\Delta\mathbf{d}$. However, only the first iteration was considered, so that $\Delta\mathbf{d} = \Delta\mathbf{d}^{(0)}$ and $\Delta\mathbf{f} = \Delta\mathbf{f}^{(1)}$. Herein, we use the iterated form for the random displacement and equivalent force vectors in Eqs. (8) and (10), which, when substituted into Eq. (11), yields

$$\begin{aligned} c &= \mathbf{f}^{\mathrm{T}}\mathbf{d} + \Delta\mathbf{d}^{\mathrm{T}}\mathbf{U}^{\mathrm{T}}\mathbf{K}_0\mathbf{U}\Delta\mathbf{d} - \frac{1}{2}\Delta\mathbf{d}^{\mathrm{T}}\mathbf{e}_i\mathbf{d}^{\mathrm{T}}\mathbf{K}_{0,ij}\mathbf{d}\mathbf{e}_j^{\mathrm{T}}\Delta\mathbf{d} \\ &= \mathbf{f}^{\mathrm{T}}\mathbf{d} + \Delta\mathbf{d}^{(0)T}\mathbf{A}^{\mathrm{T}}\mathbf{U}^{\mathrm{T}}\mathbf{K}_0\mathbf{U}\mathbf{A}\Delta\mathbf{d}^{(0)} \\ &\quad - \frac{1}{2}\Delta\mathbf{d}^{(0)\mathrm{T}}\mathbf{A}^{\mathrm{T}}\mathbf{e}_i\mathbf{d}^{\mathrm{T}}\mathbf{K}_{0,ij}\mathbf{d}\mathbf{e}_j^{\mathrm{T}}\mathbf{A}\Delta\mathbf{d}^{(0)} \end{aligned} \tag{12}$$

To obtain the expected value of the compliance, it is necessary to know the correlation structure of the random variables. Geometric randomness is generally uncorrelated in trusses by nature, and thus we express correlation in terms of the Kroneker delta as $E[\Delta X_i \Delta X_j] = \sigma_i^2\delta_{ij}$ without the summation over index i. It is useful to rewrite this in terms of the initial random displacement $\Delta\mathbf{d}^{(0)}$:

$$E[\Delta\mathbf{d}^{(0)}\Delta\mathbf{d}^{(0)\mathrm{T}}] = \mathbf{C}_0 \tag{13}$$

where $\mathbf{C}^{(\mathbf{0})}$ is the diagonal covariance matrix of the coordinate random vector with diagonal elements σ_i^2. To evaluate the expected value of the compliance, $E[c]$, it is necessary to put the random vectors together in the expression for the compliance, c. This is done by using the trace operator and by using the commutative property of matrices and vectors multiplied within the trace operator:

$$\begin{aligned} E[c] &= \mathbf{f}^{\mathrm{T}}\mathbf{d} + E\left[\mathrm{tr}\left\{\Delta\mathbf{d}^{(0)\mathrm{T}}\mathbf{A}^{\mathrm{T}}\left(\mathbf{U}^{\mathrm{T}}\mathbf{K}_0\mathbf{U} - \frac{1}{2}\mathbf{e}_i\mathbf{d}^{\mathrm{T}}\mathbf{K}_{0,ij}\mathbf{d}\mathbf{e}_j^{\mathrm{T}}\right)\mathbf{A}\Delta\mathbf{d}^{(0)}\right\}\right] \\ &= \mathbf{f}^{\mathrm{T}}\mathbf{d} + \mathrm{tr}\left\{\left(\mathbf{U}^{\mathrm{T}}\mathbf{K}_0\mathbf{U} - \frac{1}{2}\mathbf{e}_i\mathbf{d}^{\mathrm{T}}\mathbf{K}_{0,ij}\mathbf{d}\mathbf{e}_j^{\mathrm{T}}\right)\mathbf{A}E\left[\Delta\mathbf{d}^{(0)}\Delta\mathbf{d}^{(0)\mathrm{T}}\right]\mathbf{A}^{\mathrm{T}}\right\} \\ &= \mathbf{f}^{\mathrm{T}}\mathbf{d} + \mathrm{tr}\left\{\left(\mathbf{U}^{\mathrm{T}}\mathbf{F} - \frac{1}{2}\mathbf{e}_i\mathbf{d}^{\mathrm{T}}\mathbf{K}_{0,ij}\mathbf{d}\mathbf{e}_j^{\mathrm{T}}\right)\mathbf{C}\right\} \end{aligned} \tag{14}$$

where $\mathbf{F} = \mathbf{K}_0\mathbf{U} = -\mathbf{K}_{0,i}\mathbf{d}\mathbf{e}_i^{\mathrm{T}}$ is a matrix of normalized equivalent forces, and we have defined:

$$\mathbf{C} = \mathbf{A}\mathbf{C}_0\mathbf{A}^{\mathrm{T}} \tag{15}$$

2.2. Topology optimization formulation

It is now possible to express the topology optimization design problem in terms of the expected value of the compliance:

$$\min_{\boldsymbol{\rho}} E[C(\boldsymbol{\rho})] = \mathbf{f}^{\mathrm{T}}\mathbf{d} + \mathrm{tr}\left\{\left(\mathbf{U}^{\mathrm{T}}\mathbf{F} - \frac{1}{2}\mathbf{e}_i\mathbf{d}^{\mathrm{T}}\mathbf{K}_{0,ij}\mathbf{d}\mathbf{e}_j^{\mathrm{T}}\right)\mathbf{C}\right\}$$
$$\text{such that } \begin{cases} \mathbf{K}_0\mathbf{d} = \mathbf{f} \\ \mathbf{K}_0\mathbf{U} = \mathbf{F} \\ \Sigma_e\rho^e v^e \leqslant V \\ \rho^e \geqslant \rho_{\min} \end{cases} \tag{16}$$

where ρ^e is the cross-sectional area of member e stored in the vector of cross-sectional areas $\boldsymbol{\rho}$, v^e is the corresponding volume for unit magnitude of ρ^e (member length for trusses), V is the allowable volume of material, and lower bound ρ_{min} is a small positive number ($\sim 10^{-3}$). The first two equality constraints are for the equilibrium conditions under the real applied loads $\mathbf{f}$ and normalized equivalent random forces $\mathbf{F}$. The matrices $\mathbf{K}_0$, $\mathbf{K}_{0,i}$, and $\mathbf{K}_{0,ij}$ are assembled via standard finite element assembly from their respective element matrices; the expressions for these for truss elements can be found in Guest and Igusa (2008). Since these matrices are functions of $\boldsymbol{\rho}_e$, it follows that $\mathbf{A}$, $\mathbf{F}$, $\mathbf{d}$ and $\mathbf{U}$ are also functions of $\boldsymbol{\rho}$. To make the sensitivity computations for the gradient-based optimization process computationally efficient, the derivatives of the objective function with respect to $\boldsymbol{\rho}$ may be found using direct differentiation (or the adjoint method). The resulting expressions are straightforward and efficient to compute. They are, however, involved and are thus presented in the appendix.

2.3. Optimization algorithm

The above expressions are used in the design optimization algorithm as follows.

1. Initialize $\boldsymbol{\rho}$ (e.g., areas are uniformly distributed to satisfy the volume constraint).
2. Calculate the displacements $\mathbf{d}$ due to load $\mathbf{f}$ by solving $\mathbf{K}_0\mathbf{d} = \mathbf{f}$.
3. Calculate $\mathbf{F}$ and $\mathbf{U}$ using $\mathbf{F} = -\mathbf{K}_{0,i}\mathbf{d}\mathbf{e}_i^{\mathrm{T}}$ and solving $\mathbf{K}_0\mathbf{U} = \mathbf{F}$.
4. Holding the displacements fixed, calculate $\mathbf{A}$ using Eq. (9), the objective function using Eq. (14), and the sensitivity of the objective function using equation (A.13) of the Appendix.
5. Update $\boldsymbol{\rho}$ using a gradient-based optimizer.
6. If not converged, go to step 2; otherwise, $\boldsymbol{\rho}$ gives the final design.

The steps above require solution of several linear systems. However, a key advantage of the perturbation-based methodology is that each of the systems in steps 2 and 3 have the same left-hand side: the deterministic global stiffness matrix $\mathbf{K}_0$. Therefore, the solution of $\mathbf{d}$ and $\mathbf{U}$ simply require solving a linear system of equations with multiple right-hand sides (real load case $\mathbf{f}$ and equivalent load cases $\mathbf{F}$). This cost can be effectively mitigated with proper solver selection, such as L-U factorization. The primary computational difference between this new methodology and the original perturbation-based algorithm is the computation of $\mathbf{A}$.

It should be noted that topology optimization allows for the removal of structural elements. Thus, in step 5, elements that achieve a cross-sectional area below a prescribed threshold are removed from the domain and the structural connectivity is updated (see Bendsøe et al., 1994; Kirsch, 1989; Bendsøe and Sigmund, 2003).

3. Numerical examples

In this section we illustrate the effects of geometric uncertainties on the design of several truss examples using the proposed formulation. In these examples, all truss members have unit Young's modulus and total available material volume of 790 units. Sequential Quadratic Programming, as implemented in the MATLAB Optimization Toolbox, is used for the gradient-based optimizer. The examples were also solved using the Method of Moving Asymptotes (Svanberg, 1987) with no significant difference in solution quality.

3.1. Simple column

We begin with the simple ground structure shown in Fig. 1(a), also studied in Guest and Igusa (2008), with horizontal and vertical

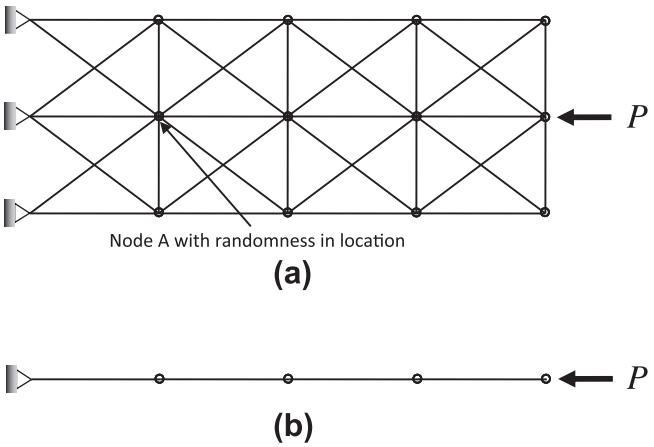

Fig. 1. Simple column example. (a) Ground structure geometry, boundary conditions and applied load, and (b) optimal solution under deterministic design conditions.

nodal spacing of 40 and 30 units, respectively. The horizontal load is applied mid-height at the right boundary, as either a compressive or tensile load. The solution for the deterministic design condition of perfectly alligned nodes is given by the four colinear bars shown in Fig. 1(b). This solution is independent of the load direction and magnitude. This structure appears efficient, but under any perturbation in nodal locations it becomes (i) kinematically unstable under a compressive applied load or (ii) inefficient under a tensile load (becoming efficient only after the bar becomes straightened under the load).

We now consider the illustrative case of randomness in a single node using the proprosed algorithm. Both spatial coordinates of node A (Fig. 1(a)) are considered uncertain, with randomness quantified by the standard deviation of σ_A in each coordinate direction. Fig. 2 displays results for a compressive load of magnitude $P = 0.15$ units with two levels of node location uncertainty: $\sigma_A = 0.1L_x$ and $0.2L_x$, where $L_x = 40$ is the length of a single horizontal truss member. The design under the smaller magnitude uncertainty, shown in Fig. 2(a), includes bracing of node A, as well as the nodes connected to node A. This is expected due to the vertical internal forces induced by the misalignment of node A. This topology is identical to the solution presented in Guest and Igusa (2008) with only minor differences in the distribution of material. The design for the larger uncertainty of $\sigma_A = 0.2L_x$, shown in Fig. 2(b), includes distributed bracing throughout the system. This is consistent with the fact that buckling is a global phenomenon. The differences in designs are algorithmically driven by the amplification matrix **A** and corresponding differences in the global equivalent forces **F**. For small uncertainties, these equivalent forces are localized around node A, and become very similar to the localized equivalent forces derived by Guest and Igusa (2008) (this explains similarity of Fig. 2(a) to their solutions). For larger uncertainties, the equivalent forces **F** become significant for nodes that are farther from node A. This global effect results in more extensive truss bracing as shown in Fig. 2(b).

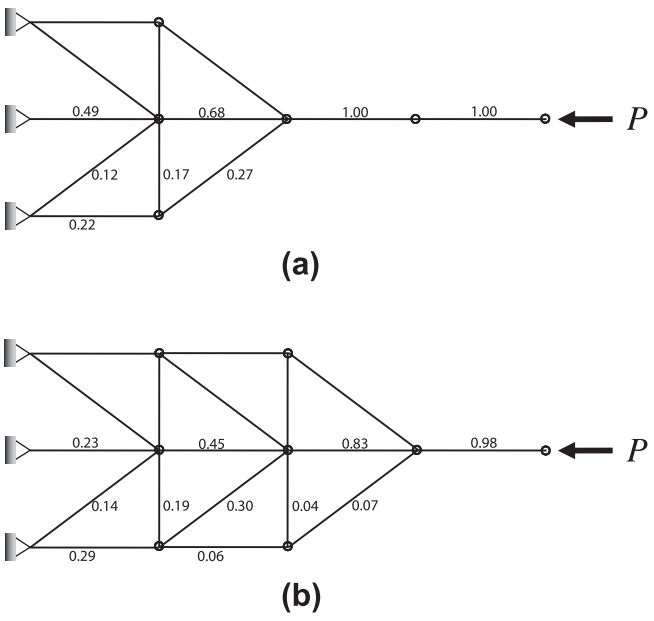

Fig. 2. Optimized design for the simple column example under compressive load P and (a) 10% variability and (b) 20% variability in location of node A. All cross-sectional areas are normalized by the maximum member area in (a).

When the applied load is changed from compression to tension, the structural designs reduce to a straight bar for both levels of randomness, as shown in Fig. 3. Analytically this is due to the fact that the global equivalent forces are dependent on the sign of the applied load. In the previous work (Guest and Igusa, 2008), the magnitudes of localized equivalent forces were independent of the sign of the applied loads due to the assumption of linear elasticity, so that the design under compression and tension were both given by Fig. 2(a).

As suggested in Eq. (16), optimal topologies are also dependent on the force magnitude. We briefly examine the changes in the design as the tensile force is reduced from P to $P/2$ and $P/3$, for the case of 20% geometric variability at node A and P of 0.15 units as before. The results, shown in Fig. 4(a) and (b), show that as the force is reduced, the bracing increases. To understand this, it is

Fig. 3. Optimized design for the simple column example under tensile load P for both 10% variability and 20% variability in location of node A.

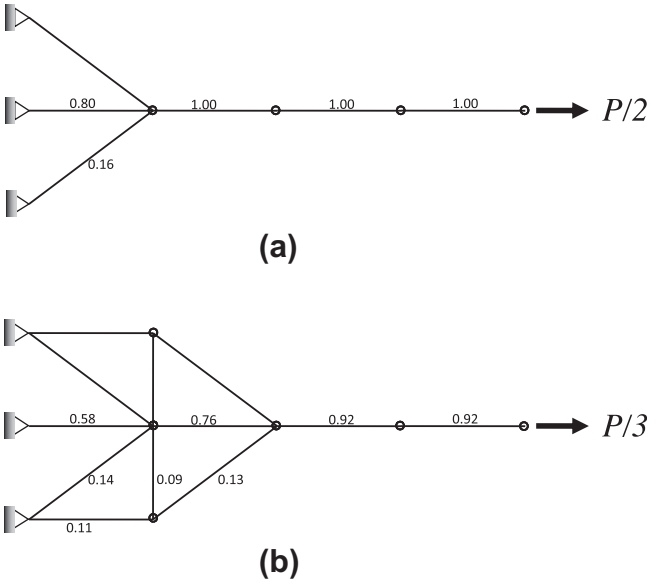

Fig. 4. Optimized design for the simple column example considering 20% variability in location of node A and tensile loading of magnitude (a) $P/2$ and (b) $P/3$. Compared to the solution under load P (Fig. 3), smaller tensile loads spur increased bracing as the perturbed middle bar can be prevented from reaching a collinear deflected state. All cross-sectional area magnitudes are normalized by the maximum area of a member in case (a).

noted that the design of Fig. 3 with geometric variability at node *A* has no axial stiffness until it reaches a collinear state. As compliance is the product of force and total displacement, this initial 'free' motion leads to increased total deflection and thus compliance. If the load is relatively is small, then it is possible to reduce the compliance by adding the bracing shown in Fig. 4(a) and (b), which reduces the tendency of the middle truss elements to become collinear. For sufficiently large loads, however, the middle elements will tend to become collinear even with bracing. Hence, the optimal design is to use all of the material in the middle elements, as shown in Fig. 3.

This simple example illustrates two important properties of the new algorithm. First, the effect of nonlinearity is evident in that solutions are dependent on both the magnitude and direction (tensile or compressive) of the applied loads. Second, geometric uncertainty is spatially propagated through structurally nonlinear behavior (such as global buckling). Additional examples are examined In the following subsections to further explore these nonlinear characteristics.

3.2. Cantilever beam, center load

The ground structure for this example is shown in Fig. 5. The load magnitude is 0.3 units and design domain dimensions are 45 and 30 units in the horizontal and vertical directions, respectively. In this example, and in all of the remaining examples of this section, the line thickness is used to indicate relative cross-sectional area.

The deterministic design (no geometric uncertainties) is shown in Fig. 6. As the figure suggests, the optimized topology would contain several segments of collinear elements, yielding a kinematically unstable structure. These collinear elements have been merged into a single element to eliminate these instabilities. This is a standard approach in topology optimization but tends to increase the length of compressive members, making them more prone to local (Euler) buckling (Zhou, 1996). This is contrasted with the non-deterministic design shown in Fig. 7, found using the proposed algorithm under the assumption of geometric variability of $\sigma = 0.05L_x$ at all nodal locations. Although every node has geometric uncertainty, the bracing is used predominantly around the regions of the structure under compressive forces, as these sections are more prone to collapse due to geometric imperfections. It is also clear that the large, primary compressive load paths in Fig. 6 have been redesigned into redundant subsystems to create alternate load paths. The compressive column and diagonal member share the same bracing, leading to an economical design. It is noted that the tensile members could be manufactured as long elements, while the compressive members would be braced, as the topology design suggests.

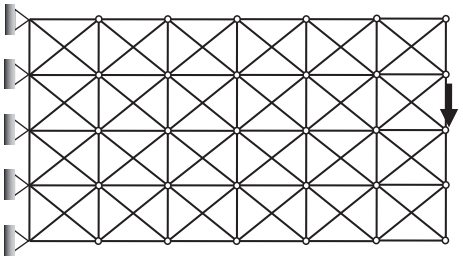

Fig. 5. Ground structure and boundary conditions for the cantilever beam example.

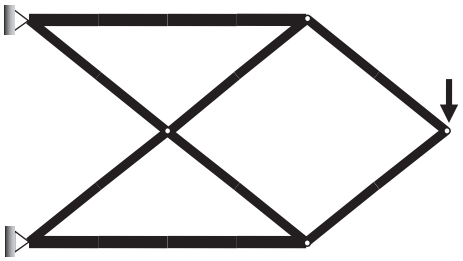

Fig. 6. Optimized cantilever design under deterministic conditions.

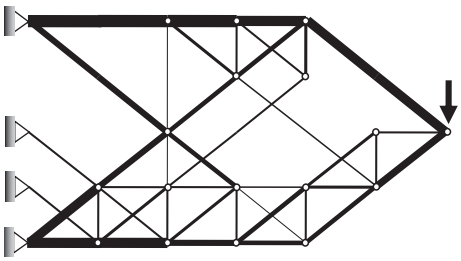

Fig. 7. Optimized cantilever design obtained using the new methodology and considering variability of 5% in all nodal locations.

We now compare the nonlinear structural performance of the deterministic and non-deterministic designs in the presence of geometric uncertainties. As mentioned, the deterministic designs contain collinear elements, and thus will fail under near-zero magnitude applied loads. To make this comparison meaningful we must merge collinear elements. Traditionally this is done by node cancelation, a process where interior nodes of the merged elements are eliminated. Such a procedure, however, would change the structural mesh and consequently the random variable field on which the topology optimization was based. Therefore, collinear elements of both designs are simply merged herein by replacing interior frictionless hinges with rigid connections. Monte Carlo simulation is used to generate a hundred independent samples for each design using uniformly distributed random node locations with zero means and standard deviation $\sigma = 0.05L_x$. Fig. 8 shows

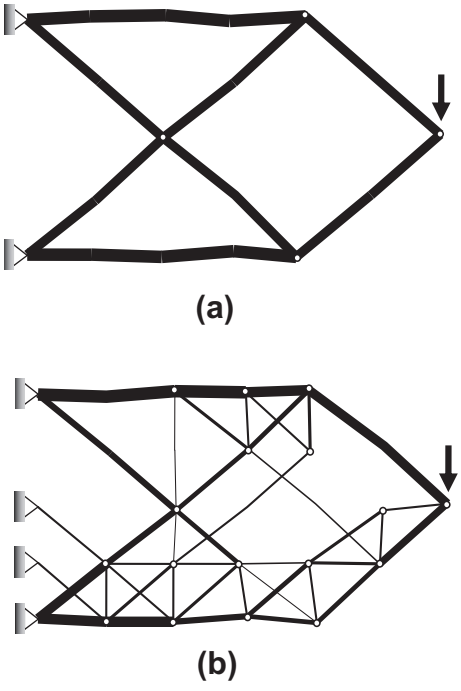

Fig. 8. One realization of the Monte Carlo generated samples for the cantilever beam structure. (a) Deterministic design and (b) design using new methodology.

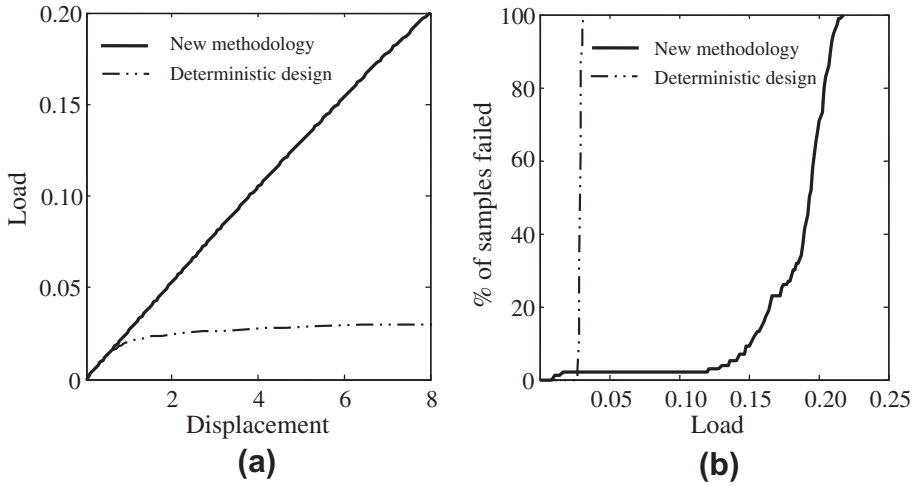

Fig. 9. Performance diagrams of the Monte Carlo generated samples using designs in Fig. 6 (deterministic) and 7 (new methodology). (a) Averaged load vs. displacement plot and (b) percentage of samples failed vs. applied load. The design found using the new methodology clearly offers improved performance when considering geometric nonlinearity and geometric imperfections.

one of these Monte Carlo samples for both designs and illustrates the presence of geometric randomness along the length of the merged elements. This is consistent with the initial ground structure geometry and represents manufacturing errors. Truss member cross-sections are assumed solid cylinders, and the load-deflection curve of each Monte Carlo sample is computed using the 2nd-order elastic analysis tool in Mastan2 software (Ziemian and McGuire, 2010).

The average of load-deflection curves is shown in Fig. 9(a), where the horizontal axis represents the vertical displacement at the location of load and the vertical axis represents the load magnitude. It can be seen that the two designs have comparable performance at low loads, but the design considering uncertainties clearly outperforms the deterministic design when the load exceeds 0.02 units. Another way to assess and compare designs is to examine the structural reliability. Here, we define structure failure as tip displacement exceeding 8 units. Fig. 9(b) displays the percentage of samples failed as a function of load magnitude. All of the samples for the deterministic design fail before the load reaches 0.032 units, while for the design considering uncertainties, only 4 of the 100 Monte Carlo samples fail at this load, all due to local (Euler) buckling. Additional failed samples do not occur until over three times this load, with 100% failure only after the load has increased by nearly a factor of six.

The relatively high second-order nonlinear performance of the non-deterministic design is due to the braced compressive load paths and the existence of multiple redundant load paths. A consequence of this design is that the structure is (on average) slightly more flexible than the deterministic solution under very small loads and deflections. This is not surprising, as the structure response is near linear elastic in this regime. Another interesting property of the design in Fig. 7 is that structure undergoes stiffening with the application of the load. This behavior can be seen in the load-displacement curve plotted in Fig. 10 for the realization shown in Fig. 7(b), and is due to the force-induced alignment of the tension members as the structure is subjected to small loads. It is noted that this increase in tangent stiffness is not as evident in the averaged curve in Fig. 9(a) as not all the realizations behave in this manner. Finally, it is noted that the irregularities in the curves of Fig. 9 are due to the relatively low number of Monte Carlo samples, and that increasing the number of samples would likely lead to smoother curves.

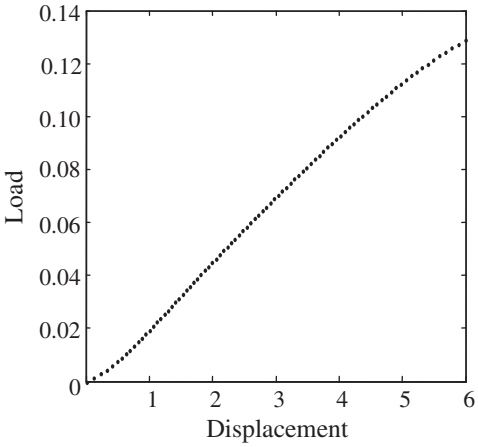

Fig. 10. Load-displacement curve for the realization shown in Fig. 8, showing structure stiffening with application of load.

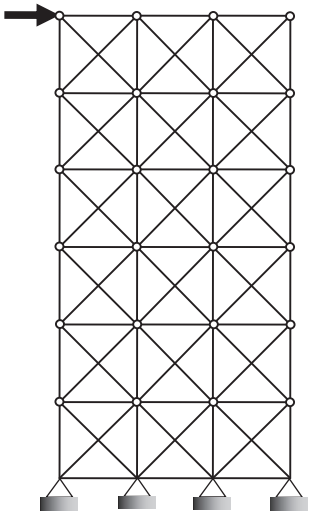

Fig. 11. Ground structure, applied load and boundary conditions for the tall cantilever example.

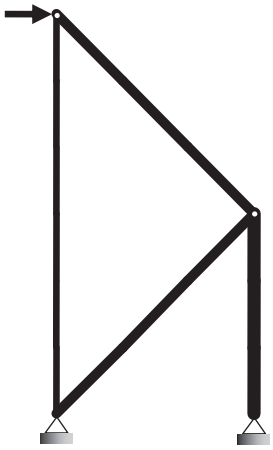

Fig. 12. Deterministic solution to the tall cantilever example.

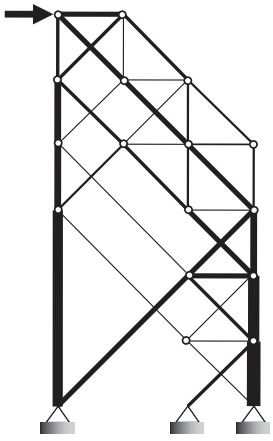

Fig. 13. Solution to the tall cantilever example obtained using the new methodology and considering randomness of 5% variability in all nodal locations.

3.3. Cantilever beam, corner load

The next example is a cantilever structure subjected to a load of 0.15 units applied at a corner, as shown in Fig. 11. The horizontal and vertical domain dimensions are 30 and 60 units,

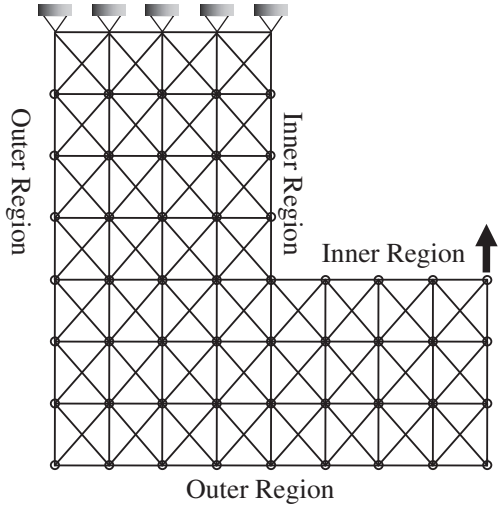

Fig. 15. Ground structure, applied loads and boundary conditions for the L-shaped structure example.

respectively. The optimized design under deterministic conditions is shown in Fig. 12, where again interior hinges have been replaced with rigid connections at the interior nodes of collinear patterns.

As in the preceding example, the design considering uncertainty assumes geometric variability of $\sigma = 0.05L_x$ at every node in the structure. The optimized design found using the proposed algorithm is shown in Fig. 13. The compressive side of the structure features multiple load paths that share a fairly dense bracing system, ultimately leading to an economical design.

To evaluate the performance of these designs in the presence of geometric uncertainties, Monte Carlo simulation is again used to generate 100 realizations of each of the designs in Figs. 12 and 13, and the load deflection curve for each realization is computed using 2nd-order elastic analysis. Averages of the load-deflection curves and the structural reliabilities of each design are shown in Fig. 14(a) and (b) in the same way they were shown in Fig. 9(a) and (b) for the preceding example. The results follow the same trends identified in the previous example: the designs created by the new methodology offer superior stiffness and lower failure rates because of the bracing and multiple load paths in the non-deterministic design.

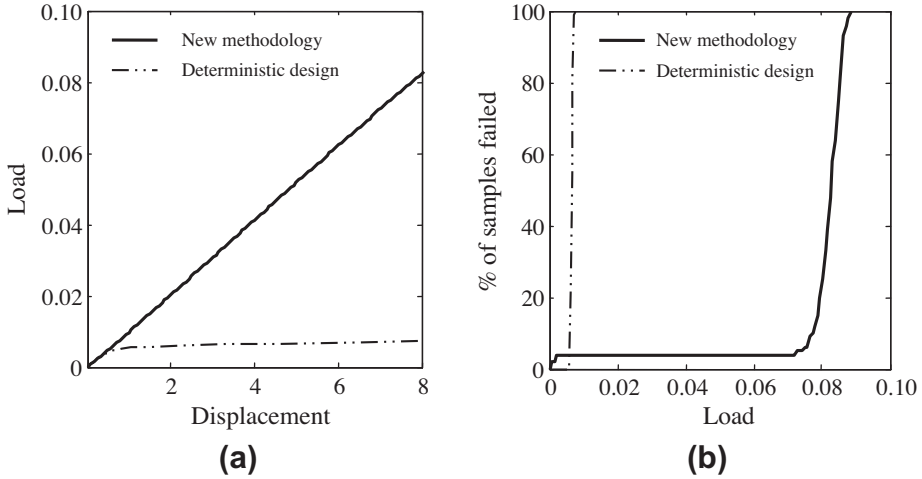

Fig. 14. Performance diagrams of the Monte Carlo generated realizations using designs in Fig. 12 (deterministic) and 13 (new methodology). (a) Averaged load vs. displacement plot and (b) percentage of samples failed vs. applied load.

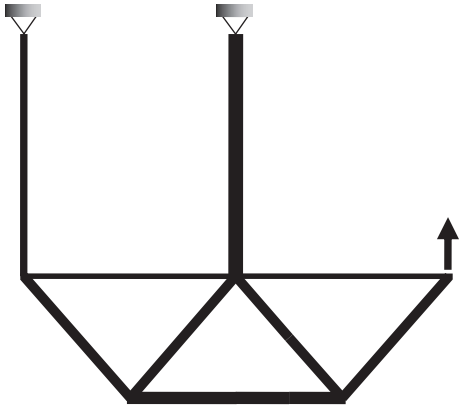

Fig. 16. Deterministic solution to the L-shaped structure example.

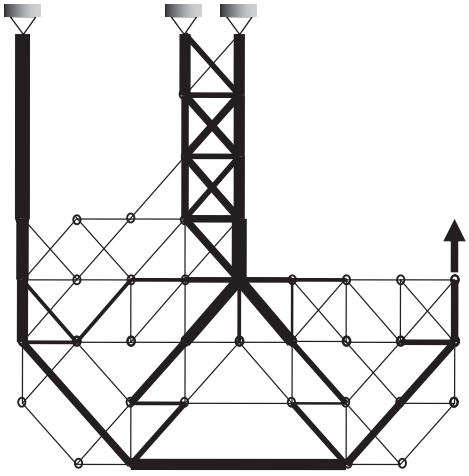

Fig. 17. Solution to the L-shaped structure example obtained using the new methodology and considering randomness in all nodal locations with 10% variability.

3.4. L-shaped structure

The final example is the L-shaped structure shown in Fig. 15. The overall dimensions are 100 by 100 units with the upper right quarter of the domain removed from the ground structure. The applied load has a magnitude of 0.1 units, leading to compression and tension zones in the inner and outer regions respectively indicated in the figure.

The optimal design under deterministic design conditions is shown in Fig. 16. Since the inner vertical member carries twice the load of the outer vertical member, the inner member is twice the cross-sectional area. Even with collinear element merging, however, the structure is kinematically unstable as it can freely rotate under any horizontal load. Fig. 17 displays the design considering geometric uncertainty assuming variability of $\sigma = 0.1L_x$ in all node locations. The tension zones receive relatively light, if any bracing, while alternate load paths and shared bracing are incorporated into the compression zones. The structure is also kinematically stable, a known byproduct of considering geometric uncertainties in truss design (Guest and Igusa, 2008).

4. Concluding remarks

This paper extends a recently developed structural optimization algorithm for design under geometric uncertainties to include a first-order approximation to geometric nonlinearities. Geometric imperfections are modeled by considering the location of truss nodes to be uncertain, which ultimately leads to uncertainty in structural stiffness. Perturbation is used to transform these uncertainties into a system of equivalent random loads. These loads are enhanced in this work to account for the increased potential of global buckling in structures with imperfections. Key characteristics of this approach not seen in the original algorithm are that (1) optimal designs are dependent on the magnitude of the load, (2) optimal designs are dependent on the direction of the load (tension or compression inducing), and (3) the impact of an uncertainty source may propagate to regions far from the source.

Several examples were considered where the goal was to minimize the expected value of compliance (maximize stiffness) in the presence of geometric uncertainties. Optimized designs consistently featured (1) compression regions with multiple load paths and shared bracing and (2) tension regions with little to no bracing, even in the presence of geometric imperfections. This more closely reflects good design practice, as tension usually cancels the effects of imperfections while compression amplifies these effects. Improved performance of the optimized solutions was also confirmed using second-order elastic analysis. Solutions found using the new methodology significantly outperformed those found under deterministic design conditions in terms of maximum load carried and stiffness in the nonlinear regime. Minimizing expected value of compliance is a first step towards robust design and it is clear that the new methodology results in designs that are less sensitive to manufacturing errors. This could significantly reduce the analysis cost in the first stages of designs, and furnishes a reliable starting point for design engineers.

A key benefit of the proposed algorithm is computational efficiency. Uncertainties in the global stiffness matrix, the left-hand side of the linear system, are transformed into equivalent loads, the right-hand side. This means we must solve, at every design iteration, a linear system with a single left-hand side and multiple right-hand sides (load cases). This is in contrast to Monte Carlo-based optimization approaches, which require, at each design iteration, solution of multiple global stiffness matrices for a single load case. The efficiency of such an approach is apparent and has been discussed in related works (Guest and Igusa, 2008; Asadpoure et al., 2011). Although the algorithm is mechanics-driven, the primary disadvantage of the proposed algorithm is that it is heuristic. The perturbation-based methodology offers mathematical equivalence in the linear elastic regime, but offers only a linear approximation to nonlinear behavior. Although the algorithm clearly produces solutions with improved nonlinear performance in the presence of geometric imperfections, the improvement in performance cannot be predicted without a full nonlinear analysis.

Acknowledgments

This work was supported by the National Science Foundation under Grant No. CMMI-0928613 with Dr. Christina Bloebaum serving as program officer. This support is gratefully acknowledged.

Appendix A. Sensitivity derivation

Consider the expected value of the minimum compliance function, which is repeated here for convenience:

$$\mathrm{E}[c] = \mathbf{f}^{\mathrm{T}}\mathbf{d} + \mathrm{tr}\left\{\left(\mathbf{U}^{\mathrm{T}}\mathbf{K}_0\mathbf{U} - \frac{1}{2}\mathbf{e}_i\mathbf{d}^{\mathrm{T}}\mathbf{K}_{0,ij}\mathbf{d}\mathbf{e}_j^{\mathrm{T}}\right)\mathbf{C}\right\} \tag{A.1}$$

In the following, primes denote the derivative with respect to design variables. Using the chain rule yields the following:

$$\mathrm{E}[c]' = \mathbf{f}^{\mathrm{T}}\mathbf{d}' + \mathrm{tr}\Big\{\Big(\mathbf{U}^{\mathrm{T}}\mathbf{K}_0'\mathbf{U} + 2\mathbf{U}^{\mathrm{T}}\mathbf{K}_0\mathbf{U}' - \mathbf{e}_i\Big(\frac{1}{2}\mathbf{d}^{\mathrm{T}}\mathbf{K}_{0,ij}'\mathbf{d} + \mathbf{d}^{\mathrm{T}}\mathbf{K}_{0,ij}\mathbf{d}'\Big)\mathbf{e}_j^{\mathrm{T}}\Big)\mathbf{C} + \mathbf{K}_{\mathrm{U}}\mathbf{C}'\Big\} \tag{A.2}$$

where we have defined:

$$\mathbf{K}_U = \mathbf{U}^{\mathrm{T}}\mathbf{K}_0\mathbf{U} - \frac{1}{2}\mathbf{e}_i\mathbf{d}^{\mathrm{T}}\mathbf{K}_{0,ij}\mathbf{d}\mathbf{e}_j^{\mathrm{T}} \tag{A.3}$$

Differentiating Eq. (15) yields:

$$\mathbf{C}' = \mathbf{A}'\mathbf{C}_0\mathbf{A}^{\mathrm{T}} + \mathbf{A}\mathbf{C}_0\mathbf{A}'^{T} \tag{A.4}$$

and differentiating Eq. (9) yields:

$$\mathbf{A}' = \mathbf{A}\mathbf{U}'\mathbf{A} \tag{A.5}$$

Combining the preceding three equations would lead us to:

$$\mathrm{tr}\{\mathbf{K}_U\mathbf{C}'\} = 2\mathrm{tr}\{\mathbf{K}_U\mathbf{A}'\mathbf{C}_0\mathbf{A}^{\mathrm{T}}\} = 2\mathrm{tr}\{\mathbf{C}\mathbf{K}_U\mathbf{A}\mathbf{U}'\} \tag{A.6}$$

Substituting (A.6) into (A.2), collecting terms, and using the trace operator properties yields:

$$\mathrm{E}[c]' = [\mathbf{f}^{\mathrm{T}} - C_{ij}\mathbf{d}^{\mathrm{T}}\mathbf{K}_{0,ij}]\mathbf{d}' + 2\mathrm{tr}\Big\{\mathbf{C}(\mathbf{U}^{\mathrm{T}}\mathbf{K}_0 + \mathbf{K}_{\mathbf{U}}\mathbf{A})\mathbf{U}'\Big\} + \mathrm{tr}\Big\{\mathbf{C}\mathbf{U}^{\mathrm{T}}\mathbf{K}_0'\mathbf{U}\Big\} - \frac{1}{2}C_{ij}\mathbf{d}^{\mathrm{T}}\mathbf{K}_{0,ij}'\mathbf{d} \tag{A.7}$$

The derivatives of the stiffness matrices with respect to the design variables are straightforward to compute (Guest and Igusa, 2008). The derivatives of the displacements **d** and **U** are found using direct differentiation. Recall that:

$$\mathbf{K}_0\mathbf{d} = \mathbf{f} \tag{A.8}$$

$$\mathbf{K}_0\mathbf{U} = -\mathbf{K}_{0,i}\mathbf{d}\mathbf{e}_i^{\mathrm{T}} \tag{A.9}$$

So we have:

$$\mathbf{d}' = -\mathbf{K}_0^{-1}\mathbf{K}_0'\mathbf{d} \tag{A.10}$$

$$\mathbf{U}' = -\mathbf{K}_0^{-1'}\mathbf{K}_{0,i}\mathbf{d}\mathbf{e}_i^{\mathrm{T}} - \mathbf{K}_0^{-1}\mathbf{K}_{0,i}'\mathbf{d}\mathbf{e}_i^{\mathrm{T}} - \mathbf{K}_0^{-1}\mathbf{K}_{0,i}\mathbf{d}'\mathbf{e}_i^{\mathrm{T}} = \mathbf{K}_0^{-1}(\mathbf{K}_0'\mathbf{K}_0^{-1}\mathbf{K}_{0,i} - \mathbf{K}_{0,i}' + \mathbf{K}_{0,i}\mathbf{K}_0^{-1}\mathbf{K}_0')\mathbf{d}\mathbf{e}_i^{\mathrm{T}} \tag{A.11}$$

Substituting the above results into (A.7) would lead us to:

$$\mathrm{E}[c]' = \Big[\mathbf{f}^{\mathrm{T}} - C_{ij}\mathbf{d}^{\mathrm{T}}\mathbf{K}_{0,ij}\Big]\mathbf{d}' - \frac{1}{2}C_{ij}\mathbf{d}^{\mathrm{T}}\mathbf{K}_{0,ij}'\mathbf{d} + 2\mathrm{tr}\Big\{\mathbf{C}(\mathbf{U}^{\mathrm{T}}\mathbf{K}_0 + \mathbf{K}_{\mathrm{U}}\mathbf{A})\Big(\mathbf{K}_0^{-1}\Big(-\mathbf{K}_0'\mathbf{U} - \mathbf{K}_{0,i}'\mathbf{d}\mathbf{e}_i^{\mathrm{T}} - \mathbf{K}_{0,i}\mathbf{d}'\mathbf{e}_i^{\mathrm{T}}\Big)\Big)\Big\} + \mathrm{tr}\Big\{\mathbf{C}\mathbf{U}^{\mathrm{T}}\mathbf{K}_0'\mathbf{U}\Big\} \tag{A.12}$$

Using the properties of trace operator and collecting terms gives the final form of the sensitivities:

$$\mathrm{E}[c]' = [\mathbf{f}^{\mathrm{T}} - C_{ij}\mathbf{d}^{\mathrm{T}}\mathbf{K}_{0,ij}]\mathbf{d}' - \mathrm{tr}\Big\{\mathbf{C}\Big(\mathbf{U}^{\mathrm{T}}\mathbf{K}_0'\mathbf{U} + 2\mathbf{K}_{\mathrm{U}}\mathbf{A}\mathbf{K}_0^{-1}\mathbf{K}_0'\mathbf{U}\Big)\Big\} - 2\mathrm{tr}\Big\{\mathbf{e}_i^{\mathrm{T}}\mathbf{C}\Big(\Big(\mathbf{U}^{\mathrm{T}} + \mathbf{K}_{\mathrm{U}}\mathbf{A}\mathbf{K}_0^{-1}\Big)\Big(\mathbf{K}_{0,i}\mathbf{d}' + \mathbf{K}_{0,i}'\mathbf{d}\Big)\Big)\Big\} - \frac{1}{2}C_{ij}\mathbf{d}^{\mathrm{T}}\mathbf{K}_{0,ij}'\mathbf{d} \tag{A.13}$$

References

Achtziger, W., 1999. Local stability of trusses in the context of topology optimization part II: a numerical approach. Structural Optimization 17, 247–258.

Achtziger, W., Bendsøe, M., Ben-Tal, A., Zowe, J., 1992. Equivalent displacement based formulations for maximum strength truss topology design. Impact of Computing in Science and Engineering 4, 315–345.

Asadpoure, A., Tootkaboni, M., Guest, J.K., 2011. Robust topology optimization of structures with uncertainties in stiffness – Application to truss structures. Computers and Structures 89, 1131–1141.

Bendsøe, M.P., Sigmund, O., 2003. Topology Optimization: Theory, Methods, and Application, Second ed. Springer, New York.

Bendsøe, M.P., Ben-Tal, A., Zowe, J., 1994. Optimization methods for truss geometry and topology design. Structural and Multidisciplinary Optimization 7, 141–159.

Ben-Tal, A., Jarre, F., Kočvara, M., Nemirovski, A., Zowe, J., 2000. Optimal design of trusses under a nonconvex global buckling constraint. Journal of Optimization and Engineering 1, 189–213.

Ben-Tal, A., Nemirovski, A., 1997. Robust truss topology design via semi definite programming. SIAM Journal on Optimization 7, 991–1016.

Calafiore, G.C., Dabbene, F., 2008. Optimization under uncertainty with applications to design of truss structures. Structural and Multidisciplinary Optimization 35, 189–200.

Cheng, G.D., Guo, X., 1997. ε-relaxed approach in structural topology optimization. Structural and Multidisciplinary Optimization 13, 258–266.

Diaz, A., Bendsøe, M.P., 1992. Shape optimization of structures for multiple loading conditions using a homogenization method. Structural and Multidisciplinary Optimization 4, 17–22.

Duysinx, P., Bendsøe, MP., 1998. Topology optimization of continuum structures with local stress constraints. International Journal for Numerical Methods in Engineering 43, 1453–1478.

Guest, J.K., Igusa, T., 2008. Structural optimization under uncertain loads and nodal locations. Computer Methods in Applied Mechanics and Engineering 198, 116–124.

Guo, X., Cheng, G., Yamazaki, K., 2001. A new approach for the solution of singular optima in truss topology optimization with stress and local buckling constraints. Structural and Multidisciplinary Optimization 22, 364–372.

Guo, X., Cheng, G.D., Olhoff, N., 2005. Optimum design of truss topology under buckling constraints. Structural and Multidisciplinary Optimization 30, 169–180.

Kirsch, U., 1989. Optimal topologies of truss structures. Computer Methods in Applied Mechanics and Engineering 72, 15–28.

Kirsch, U., 1996. Integration of reduction and expansion process in layout optimization. Structural and Multidisciplinary Optimization 11, 13–18.

Kočvara, M., 2002. On the modeling and solving of the truss design problem with global stability constraints. Structural and Multidisciplinary Optimization 23, 189–203.

Lógó, J., 2007. New type of optimality criteria method in case of probabilistic loading conditions. Mechanics Based Design of Structures and Machines 35, 147–162.

Lógó, J., Ghaemi, M., Rad, M.M., 2009. Optimal topologies in case of probabilistic loading: the influence of load correlation. Mechanics Based Design of Structures and Machines 37, 327–348.

Neves, M.M., Rodrigues, H.C., Guedes, J.M., 1995. Generalized topology design of structures with a buckling load criterion. Structural and Multidisciplinary Optimization 10, 71–78.

Rozvany, G.I.N., 1996. Difficulties in truss topology optimization with stress, local buckling and system stability constraints. Structural and Multidisciplinary Optimization 11, 213–217.

Sandgren, E., Cameron, TM., 2002. Robust design optimization of structures through consideration of variation. Computers and Structures 80, 1605–1613.

Stolpe, M., 2004. Global optimization of minimum weight truss topology problems with stress, displacement, and local buckling constraints using branch-and-bound. International Journal for Numerical Methods in Engineering 61, 1270–1309.

Svanberg, K., 1987. The method of moving asymptotes – a new method for structural optimization. International Journal for Numerical Methods in Engineering 24, 359–373.

Tyas, A., Gilbert, M., Pritchard, T., 2006. Practical plastic layout optimization of trusses incorporating stability considerations. Computers & Structures 84, 115–126.

Yonekura, K., Kanno, Y., 2010. Global optimization of robust truss topology via mixed integer semi definite programming. Optimization and Engineering 11, 355–379.

Ziemian, R.D., McGuire, W., 2010. MASTAN2, Interactive linear and nonlinear structural analysis software, distributed by John Wiley and Sons Publishers, New York, Version 1.0, 2000, Version 2.0, 2002, and Version 3.0, 2009-10 <www.mastan2.com> (last accessed April 7, 2011).

Zhou, M., 1996. Difficulties in truss topology optimization with stress and local buckling constraints. Structural and Multidisciplinary Optimization 11, 134–136.